

ZeroStereo: Zero-shot Stereo Matching from Single Images

Xianqi Wang¹, Hao Yang¹, Gangwei Xu¹, Junda Cheng¹, Min Lin¹
Yong Deng², Jinliang Zang², Yurui Chen², Xin Yang^{3,1†}

¹Huazhong University of Science and Technology ²Autel Robotics ³Optics Valley Laboratory
{xianqiw, haoyang2002, gwxu, jundacheng, minlin, xinyang2014}@hust.edu.cn



Figure 1. Zero-shot generalization results by RAFT-Stereo [25] trained under our ZeroStereo pipeline.

Abstract

State-of-the-art supervised stereo matching methods have achieved remarkable performance on various benchmarks. However, their generalization to real-world scenarios remains challenging due to the scarcity of annotated real-world stereo data. In this paper, we propose ZeroStereo, a novel stereo image generation pipeline for zero-shot stereo matching. Our approach synthesizes high-quality right images from arbitrary single images by leveraging pseudo disparities generated by a monocular depth estimation model. Unlike previous methods that address occluded regions by filling missing areas with neighboring pixels or random backgrounds, we fine-tune a diffusion inpainting model to recover missing details while preserving semantic structure. Additionally, we propose Training-Free Confidence Generation, which mitigates the impact of unreliable pseudo labels without additional training, and Adaptive Disparity Selection, which ensures a diverse and realistic disparity distribution while preventing excessive occlusion and foreground distortion. Experiments demonstrate that models trained with our pipeline achieve state-of-the-art zero-shot generalization across multiple datasets, with only a dataset volume comparable to Scene Flow. Code: <https://github.com/Windsrain/ZeroStereo>.

1. Introduction

Stereo matching is a fundamental task in computer vision that estimates depth information by identifying correspond-

ing points between stereo image pairs. By computing the disparity between matched pixels, stereo matching enables 3D scene reconstruction, which is essential for applications such as autonomous driving and robotic perception.

With the advancement of deep learning, stereo matching has shifted from traditional handcrafted feature-based approaches to data-driven methods [2, 7, 9, 25, 53, 57–59]. While deep learning-based models achieve impressive performance on standard benchmarks, they struggle to generalize to real-world scenarios due to the scarcity of annotated real-world stereo data [48]. Most models rely on synthetic datasets [29, 52] or limited real-world datasets [40, 41] which fail to cover the full diversity of real-world environments. Several approaches have been proposed to mitigate this challenge.

One direction involves learning domain-invariant feature representations from synthetic data [3, 10, 26, 38, 64]. However, a domain gap persists due to fundamental differences between synthetic and real-world data distributions. Another approach leverages self-supervised learning [45, 46], using photometric loss [11] as a proxy supervision signal on unlabeled stereo images. However, this method struggles with occlusions, ghosting artifacts, and ambiguities in ill-posed regions, while large-scale collection of high-quality stereo image pairs remains non-trivial.

In recent years, view synthesis techniques [31, 35] have emerged as a promising approach to self-supervised stereo matching. These methods generate pseudo stereo images and corresponding disparity labels from single images or

NeRF-rendered scenes. Early strategies [28, 54] employ monocular depth estimation [11, 21, 37] to derive pseudo disparity labels, followed by forward warping to synthesize the right image. However, this approach struggles with occluded regions, where missing pixels are typically filled using neighboring pixels [28] or random backgrounds [54], resulting in structural inconsistencies. To address this, NeRF-Stereo [47] has been proposed to generate stereo images from NeRF-rendered scenes. It leverages an implicit 3D representation, enabling it to synthesize occluded regions during rendering, rather than relying on post-processing heuristics. Additionally, it introduces Ambient Occlusion [33] as a confidence measure to enhance the reliability of pseudo disparity. However, NeRF-Stereo requires multi-view inputs for scene reconstruction, limiting its flexibility compared to single-image-based methods. Moreover, NeRF’s reconstruction quality for distant objects is often suboptimal, leading to degraded stereo generation in large-scale outdoor environments [8].

To overcome these challenges, we propose ZeroStereo, a novel stereo image generation pipeline for zero-shot stereo matching. Inspired by Marigold [17], we hypothesize that modern diffusion models, pre-trained on large-scale image datasets, can be effectively adapted for stereo matching. However, directly applying existing diffusion inpainting models is insufficient for stereo generation, as standard inpainting tasks do not account for the complex and structured occlusion patterns in stereo pairs. To address this, we fine-tune a diffusion inpainting model specifically for stereo image synthesis, ensuring it can handle the diverse and irregular inpainting masks encountered in occluded regions. This enables our method to recover missing background details more accurately, significantly preserving semantic consistency compared to previous heuristic filling approaches. In addition to high-quality image synthesis, training stability is another key factor in stereo matching. To mitigate the impact of unreliable pseudo disparities, we introduce Training-Free Confidence Generation, which derives confidence directly from a monocular depth estimation model. Furthermore, we propose Adaptive Disparity Selection, which dynamically adjusts the disparity distribution to prevent excessive occlusions and foreground distortions. By ensuring a wider yet realistic disparity range, this component enhances the model’s ability to generalize across diverse scenarios.

By integrating these components, ZeroStereo enables efficient and high-quality stereo image generation, leading to state-of-the-art zero-shot stereo matching. Remarkably, our method achieves this performance with a dataset volume comparable to Scene Flow [29], demonstrating its ability to generate highly effective training data without requiring large-scale real-world stereo pairs.

Our main contributions can be summarized as follows:

- We propose a novel stereo image generation pipeline ZeroStereo for zero-shot stereo matching, including a fine-tuned diffusion inpainting model adapting for complex inpainting masks in stereo matching.
- We propose Training-Free Confidence Generation and Adaptive Disparity Selection to improve stereo training stability and enhance disparity diversity.
- We demonstrate that models trained with our pipeline achieve state-of-the-art zero-shot generalization performance using only a synthesized dataset volume comparable to Scene Flow.

2. Related Work

Deep Stereo Matching. The advancement of deep learning has significantly improved stereo matching. Early methods [2, 6, 42], such as DispNet [29] and GC-Net [18], employed CNNs to construct cost volumes over a predefined disparity range. More recently, iterative refinement-based methods [25, 57, 58, 60], inspired by RAFT [44], have been introduced to iteratively update disparity predictions, improving accuracy and robustness. Additionally, transformer-based models [13, 22] leverage self-attention mechanisms to capture long-range feature dependencies, enabling more effective cost volume aggregation.

Zero-shot Generalization in Stereo Matching. Despite these advancements, deep stereo models often struggle with generalization to real-world scenarios. DSMNet [64] addresses domain shifts by introducing domain normalization layers and non-local graph-based filters to enhance feature robustness. GraftNet [26] improves generalization by incorporating pre-trained features from large-scale datasets, while ITSA [10] mitigates shortcut learning using an information-theoretic approach. Inspired by masked representation learning, Rao et al. [38] propose a masking-based strategy to enhance stereo feature learning. Another line of research focuses on self-supervised learning using unlabeled images. Luo et al. [28] pioneers single-view stereo training on the KITTI dataset, while MfS-Stereo [54] generates stereo pairs from monocular images to enable training without ground-truth disparities. NeRF-Stereo [47] introduces NeRF to generate stereo images from 3D scene reconstructions.

Diffusion Models for Image Synthesis. Denoising Diffusion Probabilistic Models (DDPMs) [15] have demonstrated success in image synthesis by progressively refining images through a denoising process. Latent Diffusion Models (LDMs) [39] further improve efficiency by performing diffusion steps in a lower-dimensional latent space. ControlNet [66] extends these models by introducing spatial conditioning mechanisms for better control over generated content. RePaint [27] proposes an inpainting method based on pre-trained DDPMs, showcasing the effectiveness of diffusion models in restoring missing visual details.

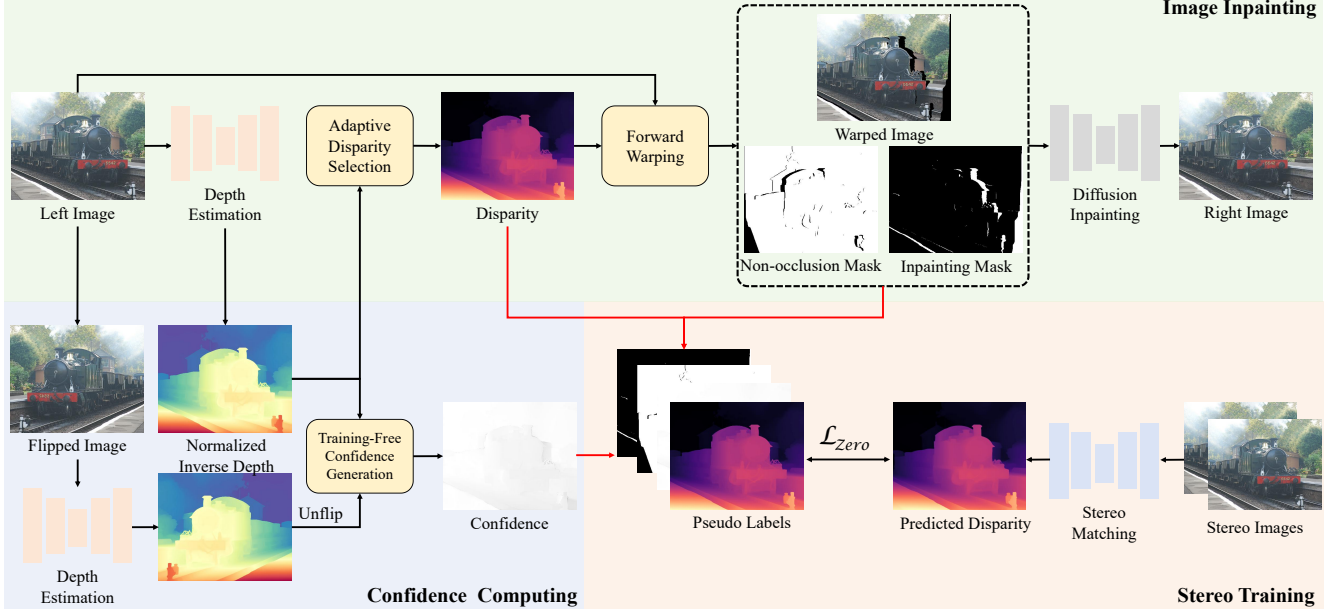


Figure 2. Overview of ZeroStereo. Given a left image, a monocular depth estimation model infers the normalized inverse depth. Our Training-Free Confidence Generation (Sec. 3.3) and Adaptive Disparity Selection (Sec. 3.4) modules extract the confidence and pseudo disparity. Forward warping is then applied to generate a warped image and corresponding masks, which are processed by a diffusion inpainting model (Sec. 3.2) to synthesize the right image. The final stereo images and pseudo labels are used for stereo training (Sec. 3.5).

3. Method

In this section, we present the overview of our ZeroStereo pipeline (Fig. 2) and details of our proposed modules.

3.1. Overview

Given a single image as the left image I_L , we first obtain a normalized inverse depth map D using a monocular depth estimation model (we use Depth Anything V2 [63], referred to as DAv2). This depth map is then converted into a pseudo disparity map d via our Adaptive Disparity Selection (ADS) module. Using the forward warping technique from [54], we generate a warped image \tilde{I}_r , a non-occlusion mask M_{noc} (pixels only visible in I_L), and an inpainting mask M_{inp} (pixels invisible in I_L). \tilde{I}_r and M_{inp} are then processed by a fine-tuned diffusion inpainting model to synthesize a high-quality right image I_r . To improve training stability, we introduce the Training-Free Confidence Generation (TCG) module, which computes confidence C . Finally, the synthesized stereo image pairs and associated pseudo labels are used to train stereo matching models.

3.2. Image Inpainting

We fine-tune a diffusion inpainting model based on Stable Diffusion V2 Inpainting (SDv2I) [39]. Although the pre-trained inpainting model can be directly applied, it is not specifically designed for stereo image synthesis. There exist differences between standard image inpainting and image inpainting in stereo matching.

First, there is no explicit textual guidance for inpainting. As a text-to-image model, SDv2I is trained on both text-conditioned and unconditioned data. However, no reliable textual prompt effectively directs the model to inpaint occluded regions in stereo matching. Second, unlike standard image inpainting, which typically restores or replaces specific objects or regions, occlusion masks in stereo matching exhibit diverse and irregular shapes. As a result, directly applying a pre-trained model yields suboptimal performance, necessitating fine-tuning to achieve effective results.

Fine-tuning Protocol. For fine-tuning, we utilize synthetic stereo datasets like Scene Flow [29] which provide dense disparity maps as ground truth. Similar to Marigold [17], synthetic data is essential because it offers dense and complete ground truth, enabling per-pixel warping. Moreover, synthetic images are free from real-world noise, ensuring cleaner training data. Given a warped image \tilde{I}_r , an inpainting mask M_{inp} , and a right image I_R , we employ a frozen Variational Auto-Encoder (VAE) [19] to encode \tilde{I}_r and I_R into the latent space. The inpainting mask M_{inp} is resized to match the latent space resolution. We then sample Gaussian noise ϵ and add it to the latent right image. Finally, these latent features and the resized inpainting mask are concatenated as input to the U-Net, which predicts noise $\tilde{\epsilon}$. The network is optimized using an L2 loss function:

$$\mathcal{L}_u = \|\tilde{\epsilon} - \epsilon\|_2^2 \quad (1)$$

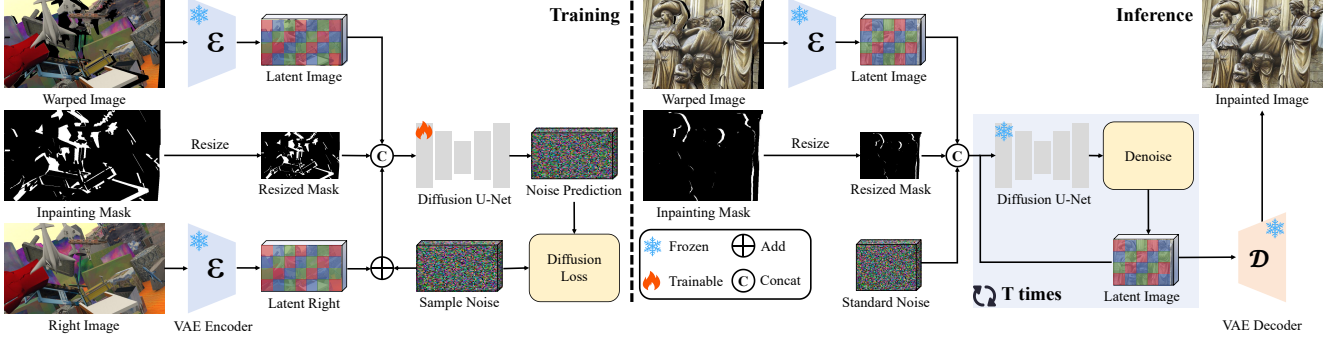


Figure 3. Overview of our diffusion inpainting protocol. During training, we freeze VAE and only fine-tune U-Net.

Inference Protocol. Given a warped image \tilde{I}_r and an inpainting mask M_{inp} , we first encode them into the latent space. Next, we sample standard Gaussian noise to initialize the latent right image and concatenate it with the encoded inputs for the U-Net. During inference, we iteratively denoise the latent representation over T steps. Finally, the VAE decoder reconstructs the denoised image I_d , yielding the final inpainted image I_r :

$$I_r = M_{inp} \odot I_d + (1 - M_{inp}) \odot \tilde{I}_r \quad (2)$$

3.3. Training-Free Confidence Generation

Assessing confidence in depth predictions remains challenging for previous monocular depth estimation models, which require additional training or auxiliary modules. Some post-processing methods rely on gradients [16] or probabilistic distributions [56] to estimate uncertainty.

Modern monocular depth estimation models [23, 62, 63] tend to predict relative depth, often represented as inverse depth in disparity space. This representation captures the relative distances between pixels, independent of camera parameters. Therefore, when an image is flipped horizontally, the predicted relative depth between pixels is expected to remain unchanged.

Given a left image I_l , we apply a horizontal flip operation $H(x)$ to obtain the flipped image I'_l . Both images are then processed separately by the monocular depth estimation model to generate their respective relative depth maps. Since we use DAv2 [63], which does not impose constraints on its predicted depth range, we normalize these outputs into the normalized inverse depth maps D and D' . The confidence C of D is then measured:

$$u = 1 - |D - H^{-1}(D')|$$

$$C = \frac{u - \min(u)}{\max(u) - \min(u)} \quad (3)$$

As shown in Fig. 4, low-confidence regions typically appear along edges, textureless areas, and thin objects, which are also ambiguous in stereo matching. These unreliable labels are suppressed to mitigate their impact on learning.

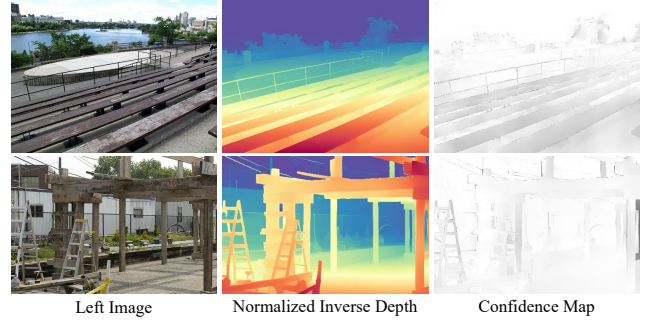


Figure 4. Visualization of confidence map.

3.4. Adaptive Disparity Selection

The previous method, MfS-Stereo [54], generates disparity maps by uniformly sampling the maximum disparity value from the range $[d_{min}, d_{max}]$. However, this fixed-range approach introduces several limitations.

First, when the image resolution is low, the disparity-to-width ratio becomes relatively large, potentially causing foreground distortion during forward warping or failure in the diffusion inpainting model due to excessive occlusion. Second, when the image resolution is high, the disparity-to-width ratio becomes relatively small, reducing the perceptible differences between the left and right images.

Therefore, we compute the disparity map d by multiplying D with the scaling factor $s \cdot w$, where w represents the image width and s is sampled from the distribution:

$$s \in \begin{cases} (c - 2r, c - r), & p = p_s \\ (c - r, c + r), & p = p_c \\ (c + r, c + 2r), & p = p_l \end{cases} \quad (4)$$

where c is the center, r is the radius, and p_i ($i \in \{s, c, l\}$) is the probability. This sampling strategy ensures that most warped images maintain high-quality while occasionally introducing extreme disparity values to enhance the robustness of stereo training. Furthermore, since single-image datasets vary in resolution, this approach allows for the generation of large disparities, effectively covering a wide range of scenarios.

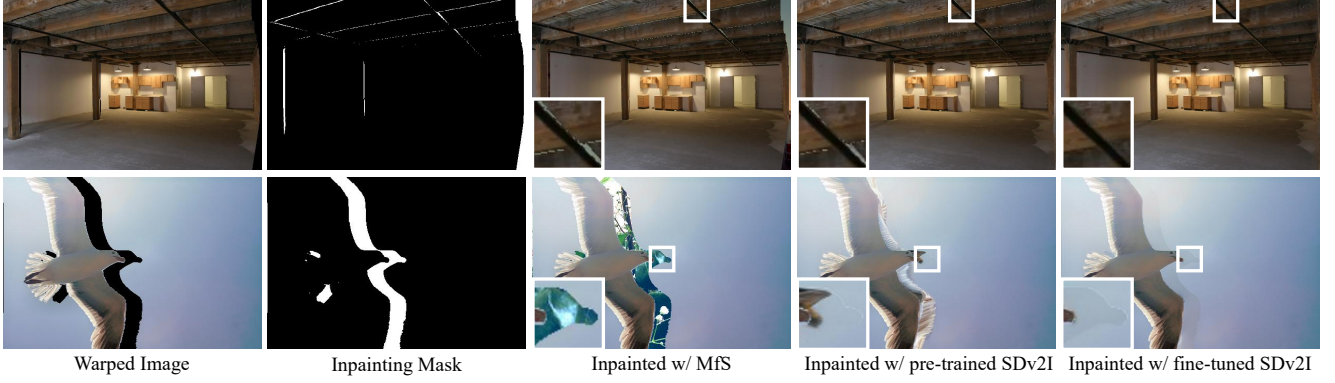


Figure 5. Visualization of different inpainting methods.



Figure 6. Visualization of StereoDiffusion [51] and our fine-tuned SDv2I.

3.5. Stereo Training

Given a stereo pair (I_l, I_r), a disparity map d , a confidence map C , a non-occlusion mask M_{noc} , an inpainting mask M_{inp} , and an estimated disparity map \tilde{d} , we train stereo matching models using our proposed ZeroStereo loss.

Disparity Loss. We adopt the same L1 loss as used in previous supervised stereo matching methods:

$$\mathcal{L}_d = \|\tilde{d} - d\|_1 \quad (5)$$

Non-occlusion Photometric Loss. We backward warp I_r using the estimated disparity \tilde{d} to obtain I_l^r . The ordinary photometric loss is then computed as:

$$\mathcal{L}_p = \beta \cdot \frac{1 - SSIM(I_l, I_l^r)}{2} + (1 - \beta) \cdot \|I_l - I_l^r\|_1 \quad (6)$$

I_l^r includes pixels inpainted by the diffusion inpainting model. To exclude these pixels, we backward warp $1 - M_{inp}$ to obtain \tilde{M}_{inp}^r . Besides, I_l^r contains ghosting artifacts due to backward warping, which we filter using M_{noc} . Thus, our loss is computed as follows:

$$\mathcal{L}_{np} = M_{noc} \odot \tilde{M}_{inp}^r \odot \mathcal{L}_p \quad (7)$$

ZeroStereo Loss. The above two terms are summed as:

$$\mathcal{L}_{Zero} = C \odot \mathcal{L}_d + \mu \cdot (1 - C) \odot \mathcal{L}_{np} \quad (8)$$

4. Experiments

In this section, we present our implementation details, evaluation datasets, ablation study, and experimental results.

4.1. Implementation Details

All experiments are implemented with PyTorch on NVIDIA RTX 4090 GPUs.

Diffusion Inpainting Model Fine-tuning. We utilize the Stable Diffusion V2 Inpainting (SDv2I) [39], disabling text conditioning and applying the DDPM noise scheduler [15] with 1,000 diffusion steps. We use a collection of synthetic stereo datasets, including Tartan Air [52], CREStereo Dataset [20], Scene Flow [29], VKITTI 2 [1], etc. Fine-tuning takes 50K steps with a batch size of 32

Baseline	ADS	Inpainting	TCG	\mathcal{L}_{Zero}	KITTI-15 All		Midd-T (H) Noc		ETH3D Noc	
					EPE	>3px	EPE	>2px	EPE	>1px
✓					1.52	4.89	2.71	8.41	0.25	2.38
	✓				1.24	4.84	2.28	7.46	0.28	2.27
		✓			1.44	4.85	2.34	7.59	0.23	1.92
			✓		1.09	4.78	2.13	7.27	0.27	2.16
	✓	✓			1.06	4.74	2.26	6.68	0.23	2.05
	✓	✓	✓		1.05	4.71	2.18	7.11	0.23	2.01
	✓	✓	✓	✓	1.04	4.73	2.09	7.07	0.22	1.90

Table 1. Ablation study of proposed modules trained with IGEV-Stereo [58]. Baseline denotes that we train the model under the pipeline in [54]. ADS denotes our Adaptive Disparity Selection module and TCG denotes our Training-free Confidence Generation module.

Dataset	DiW	COCO	DIODE	ADE20K	Mapillary
Mean	18.89	20.70	33.83	31.06	81.34
Max	75.00	96.00	153.45	627.54	751.54

Table 2. Disparity statistics results based on ADS.

Method	KITTI-15 All		Midd-T (H) Noc		ETH3D Noc	
	EPE	>3px	EPE	>2px	EPE	>1px
Pre-trained	1.18	4.77	2.27	7.21	0.25	1.90
Fine-tuned	1.06	4.74	2.26	6.68	0.23	2.05

Table 3. Ablation study of SDv2L.

Method	Resolution (px)	Memory (G)	Time (s)
RePaint [27]	256 × 256	2.7	156.5
StereoDiffusion [51]	512 × 512	14.6	31.2
Ours	512 × 512	5.8	1.9

Table 4. Ablation study of different synthesis methods.

(gradient accumulation for 4 steps). We use the AdamW optimizer and a one-cycle learning rate schedule with a learning rate of $2e-5$. Besides, we apply a crop size of 512×512 and symmetric color augmentation.

Stereo Image Generation. We use the DDIM scheduler [43] and perform 50 sampling steps. Following MfS-Stereo [54], we sample images from Depth in the Wild [4], COCO 2017 [24], DIODE [50], ADE20K [68], and Mapillary Vistas [34]. We randomly sample 35K to create a dataset called MfS35K. For disparity generation, we set: $c = 0.1$, $r = 0.05$, $p_c = 0.8$, and $p_s = p_l = 0.1$.

Stereo Matching Model Training. We use RAFT-Stereo [25] and IGEV-Stereo [58]. Models are trained on MfS35K with a batch size of 8 and a crop size of 384×512 . We follow all the source codes’ settings and train 200k steps from scratch. In addition to the data augmentation from RAFT-Stereo, we introduce Gaussian augmentation on the right image, as done in MfS-Stereo [54]. For ZeroStereo loss, we set $\beta = 0.85$, $\mu = 0.1$ the same as NeRF-Stereo [47].

4.2. Evaluation Datasets

KITTI 2015 [30] includes 200 training pairs with lidar ground truth for outdoor driving scenarios. **ETH3D** [41] contains 27 training pairs of grayscale images, covering out-

Dataset	Size	KITTI-15 >3px	Midd-T >2px	ETH3D >1px
Falling Things [49]	62K	5.14	5.81	28.63
CREStereo [20]	200K	6.26	10.91	2.56
Tartan Air [52]	307K	4.91	5.47	2.69
FoundationStereo [55]	1106K	4.69	5.11	2.52
MfS35K (Ours)	35K	4.53	4.45	2.13

Table 5. Ablation study of datasets.

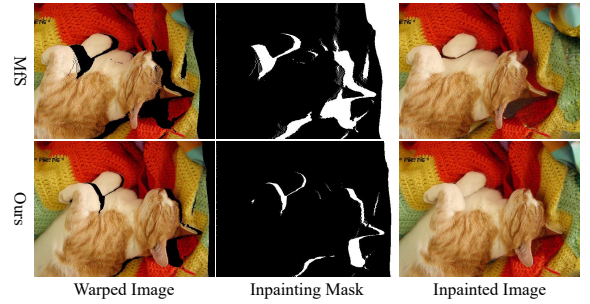


Figure 7. Visualization of different disparity selection.

door and indoor scenarios. For **Middlebury** [40], we select the Middlebury V3 Benchmark Training Set (Midd-T), which consists of 15 training pairs for high-resolution indoor scenarios.

4.3. Ablation Study

In this section, we evaluate models with different settings to verify the effectiveness of our proposed pipeline.

Effectiveness of proposed modules. Tab. 1 shows the ablation study of our proposed modules. By adding ADS or TCG, we observe a notable reduction in EPE for both KITTI-15 and Midd-T. ADS improves the model’s ability to handle large disparities. As shown in Tab. 2, the disparity range adjusts adaptively according to the dataset resolution. TCG suppresses unreliable labels, particularly in edges and textureless regions. However, adding Inpainting alone results in only a slight improvement. As shown in Fig. 7, the large disparity ratio causes separation and distortion in the foreground, which hinders the effectiveness of the diffusion inpainting model. When ADS is combined with Inpainting, we observe a significant performance improvement.

Method	KITTI-15		Midd-T				ETH3D	
	>3px		F (>2px Noc)		H (>2px Noc)		>1px	
	All	Noc	D < 192	D < All	D < 192	D < All	All	Noc
NS-IGEV-Stereo	5.88	5.58	15.89	27.91	8.55	10.67	4.02	3.58
Zero-IGEV-Stereo (Ours)	4.73	4.57	13.03	26.78	4.73	7.07	2.64	1.90
NS-RAFT-Stereo [‡] [47]	5.41	5.23	16.61	12.04	6.40	6.45	2.95	2.55
NS-RAFT-Stereo	5.65	5.44	15.05	13.41	9.09	9.44	3.30	2.79
Zero-RAFT-Stereo (Ours)	4.53	4.33	9.51	8.36	4.21	4.45	2.75	2.13

Table 6. Comparison with NeRF-Stereo [47]. Models are trained with the same augmentation. Exception: [‡] official weights.



Figure 8. Visualization of Middlebury, including Midd-T, 2014 and 2021.

Dataset	KITTI-15 All		Midd-T Noc		ETH3D Noc	
	EPE	>3px	EPE	>2px	EPE	>1px
Scene Flow [29]	1.44	8.17	2.49	15.81	0.29	3.79
NS65K [47]	1.39	7.60	2.24	11.99	0.32	4.58
MfS35K (Ours)	1.37	7.41	2.35	11.92	0.24	3.38

Table 7. Analysis of errors on edge (RAFT-Stereo).

When ADS, Inpainting, and TCG are all added, the performance consistently improves. Moreover, by introducing the final ZeroStereo Loss, the model can learn with \mathcal{L}_{Zero} in low-confidence regions. This loss helps maintain the model’s robustness, enabling it to achieve optimal performance across various datasets. A more detailed analysis can be found in our supplementary materials.

Effectiveness of fine-tuned SDv2I. As shown in Fig. 5, pixels inpainted using our fine-tuned SDv2I preserve minimal noise and maintain the semantic structure closest to the background. As shown in Tab. 3, the fine-tuned SDv2I outperforms the pre-trained model. It suggests that fine-tuning enhances the inpainting model’s ability to capture the semantic structure of the background more accurately.

Comparison with other synthesis methods. StereoDiffusion [51] introduces a training-free method for generating stereo images using the pre-trained SDv2. However, the inherent inconsistency arises because the warping oper-

ation is performed in the latent space. As shown in Fig. 6, StereoDiffusion suffers from structural distortions, texture inconsistencies, and poor occlusion handling, leading to unrealistic right-image generation. As shown in Tab. 4, our fine-tuned SDv2I is significantly faster and more memory-efficient than StereoDiffusion [51], while still achieving high-resolution synthesis. A more detailed discussion is available in our supplementary materials.

Comparison with other synthetic datasets. In recent years, many synthetic datasets with better diversity and rendering realism have been proposed. As shown in Tab. 5, our MfS35K outperforms others, despite being significantly smaller. It reveals that rather than the absolute size of datasets, the diversity of scenarios is more beneficial for zero-shot generalization.

4.4. Comparison with NeRF-Stereo

We compare our method with NeRF-Stereo [47], a leading method for generating stereo images. As shown in Tab. 6, all models are trained with the same data augmentation, except for NS-RAFT-Stereo[‡], which uses official weights. Since the official IGEV-Stereo limits \mathcal{L}_d supervision to a disparity of 192, we split the Midd-T table by disparity to provide a more detailed evaluation.

Method	KITTI-15		Middle-T						ETH3D	
	>3px		F (>2px)		H (>2px)		Q (>2px)		>1px	
	All	Noc	All	Noc	All	Noc	All	Noc	All	Noc
Training Set			Scene Flow with GT							
DSMNet [64]	5.50	5.19	41.96	38.54	18.74	14.49	13.75	9.44	4.03	3.62
CFNet [42]	5.99	5.79	35.21	30.05	21.99	17.69	14.21	10.51	6.08	5.48
Graft-PSMNet [26]	5.34	5.00	39.92	36.30	17.65	13.36	13.92	9.23	11.43	10.70
ITSA-CFNet [10]	4.73	4.67	34.01	30.14	16.48	12.32	12.28	8.54	5.43	5.17
HVT-PSMNet [3]	4.84	4.63	40.74	37.60	15.66	12.55	10.12	7.00	6.07	5.65
RAFT-Stereo [25]	5.47	5.27	15.63	11.94	11.20	8.66	10.25	7.44	2.60	2.29
IGEV-Stereo [58]	6.03	5.76	30.94	28.98	11.90	9.45	8.88	6.20	4.04	3.60
NMRF-Stereo [12]	5.31	5.14	37.63	35.25	13.36	10.90	7.87	5.07	3.80	3.48
Mocha-Stereo [5]	5.97	5.73	30.23	28.26	10.18	9.45	7.96	4.87	4.02	3.47
DKT-RAFT [65]	4.95	4.74	16.05	9.26	10.18	6.10	10.39	6.64	2.77	2.53
Former-RAFT [67]	5.18	4.93	-	-	13.27	10.29	8.51	5.61	3.96	3.50
Training Set			Real-world data without GT							
MfS-PSMNet [54]	5.18	4.91	26.42	20.91	17.56	13.45	12.07	9.09	8.17	7.44
NS-RAFT-Stereo [47]	5.41	5.23	16.38	12.04	9.70	6.45	8.09	4.85	2.95	2.55
Zero-IGEV-Stereo (Ours)	4.73	4.57	29.47	26.78	9.71	7.07	7.07	4.46	2.64	1.90
Zero-IGEV-Stereo* (Ours)	4.89	4.73	18.83	14.87	8.45	5.54	6.99	4.38	2.85	2.00
Zero-RAFT-Stereo (Ours)	4.53	4.33	12.40	8.36	7.86	4.45	7.24	4.50	2.75	2.13

Table 8. Zero-shot generalization benchmark. DKT-RAFT [65] is trained on SceneFlow [29] and fine-tuned on Booster [36]. Zero-IGEV-Stereo* denotes that we expand the \mathcal{L}_d supervision same as RAFT-Stereo [25]. We highlight **first**, **second**, **third** bests.

Re-training NS-RAFT-Stereo with our data augmentation shows no improvement, confirming that the gains are not solely due to augmentation. Zero-RAFT-Stereo outperforms NS-RAFT-Stereo[‡] by over 20%, with only a 10% drop in Middle-T (F) for $D < 192$, whereas NS-RAFT-Stereo[‡] declines more, likely due to its dataset’s imperfect reconstruction of distant objects. Fig. 8 highlights NS-RAFT-Stereo’s failures in textureless regions, while our Zero-RAFT-Stereo shows over 40% improvement in handling such cases. Moreover, as shown in Tab. 7, the model trained on MfS35K surpasses both the synthetic SceneFlow [29] and the NeRF-based NS65K [47], achieving the lowest edge error and superior edge accuracy.

4.5. Zero-shot Generalization Benchmark

Following NeRF-Stereo [47], we construct a zero-shot generalization benchmark. All methods are evaluated across the entire disparity range. For Zero-IGEV-Stereo, we train two versions: one using the original code settings for disparity supervision, and the other expanding the supervised range, consistent with RAFT-Stereo [25].

As shown in Tab. 8, our models demonstrate state-of-the-art zero-shot generalization performance across multiple datasets, both under the SceneFlow with ground truth (GT) and Real-world data without GT. Notably, Zero-RAFT-Stereo achieves the best or near-best results, particularly excelling in handling complex, real-world scenes.

Zero-IGEV-Stereo*, with an expanded supervised range of \mathcal{L}_d , shows improved results on Middlebury’s large-disparity scenarios, although this leads to a slight performance trade-off on other datasets.

5. Conclusion

We propose ZeroStereo, a novel stereo data generation pipeline for zero-shot stereo matching. The fine-tuned SDv2I adapts to complex inpainting masks and recovers background details. To handle unreliable pseudo labels, the TCG module leverages the spatial invariance of relative depth to compute confidence, helping to suppress uncertain labels. Besides, the ADS module generates a broader disparity distribution while avoiding foreground distortion. Finally, experiments demonstrate that our models achieve state-of-the-art zero-shot generalization performance.

Limitations. The fine-tuned SDv2I still struggles in some complex scenarios, and there may be occasional color inconsistencies due to fine-tuning on synthetic datasets. Furthermore, forward warping performs poorly in ill-posed regions, such as transparent areas or net-like objects.

Acknowledgement. This research is supported by the National Key R&D Program of China (2024YFE0217700), National Natural Science Foundation of China (62472184, 623B2036), the Fundamental Research Funds for the Central Universities, and the Innovation Project of Optics Valley Laboratory (Grant No. OVL2025YZ005).

References

- [1] Yohann Cabon, Naila Murray, and Martin Humenberger. Virtual kitti 2. *arXiv preprint arXiv:2001.10773*, 2020. 5
- [2] Jia-Ren Chang and Yong-Sheng Chen. Pyramid stereo matching network. In *Proceedings of the IEEE conference on computer vision and pattern recognition*, pages 5410–5418, 2018. 1, 2
- [3] Tianyu Chang, Xun Yang, Tianzhu Zhang, and Meng Wang. Domain generalized stereo matching via hierarchical visual transformation. In *Proceedings of the IEEE/CVF Conference on Computer Vision and Pattern Recognition*, pages 9559–9568, 2023. 1, 8
- [4] Weifeng Chen, Zhao Fu, Dawei Yang, and Jia Deng. Single-image depth perception in the wild. *Advances in neural information processing systems*, 29, 2016. 6
- [5] Ziyang Chen, Wei Long, He Yao, Yongjun Zhang, Bingshu Wang, Yongbin Qin, and Jia Wu. Mocha-stereo: Motif channel attention network for stereo matching. In *Proceedings of the IEEE/CVF Conference on Computer Vision and Pattern Recognition*, pages 27768–27777, 2024. 8
- [6] Junda Cheng, Xin Yang, Yuechuan Pu, and Peng Guo. Region separable stereo matching. *IEEE Transactions on Multimedia*, 25:4880–4893, 2022. 2
- [7] Junda Cheng, Gangwei Xu, Peng Guo, and Xin Yang. Coatsnet: Fully exploiting convolution and attention for stereo matching by region separation. *International Journal of Computer Vision*, 132(1):56–73, 2024. 1
- [8] Junda Cheng, Wei Yin, Kaixuan Wang, Xiaozhi Chen, Shijie Wang, and Xin Yang. Adaptive fusion of single-view and multi-view depth for autonomous driving. In *Proceedings of the IEEE/CVF Conference on Computer Vision and Pattern Recognition*, pages 10138–10147, 2024. 2
- [9] Junda Cheng, Longliang Liu, Gangwei Xu, Xianqi Wang, Zhaoxing Zhang, Yong Deng, Jinliang Zang, Yurui Chen, Zhipeng Cai, and Xin Yang. Monster: Marry monodepth to stereo unleashes power. *arXiv preprint arXiv:2501.08643*, 2025. 1
- [10] WeiQin Chuah, Ruwan Tennakoon, Reza Hoseinnezhad, Alireza Bab-Hadiashar, and David Suter. Itsa: An information-theoretic approach to automatic shortcut avoidance and domain generalization in stereo matching networks. In *Proceedings of the IEEE/CVF Conference on Computer Vision and Pattern Recognition*, pages 13022–13032, 2022. 1, 2, 8
- [11] Clément Godard, Oisín Mac Aodha, Michael Firman, and Gabriel J Brostow. Digging into self-supervised monocular depth estimation. In *Proceedings of the IEEE/CVF international conference on computer vision*, pages 3828–3838, 2019. 1, 2
- [12] Tongfan Guan, Chen Wang, and Yun-Hui Liu. Neural markov random field for stereo matching. In *Proceedings of the IEEE/CVF Conference on Computer Vision and Pattern Recognition*, pages 5459–5469, 2024. 8
- [13] Weiyu Guo, Zhaoshuo Li, Yongkui Yang, Zheng Wang, Russell H Taylor, Mathias Unberath, Alan Yuille, and Yingwei Li. Context-enhanced stereo transformer. In *European Conference on Computer Vision*, pages 263–279. Springer, 2022. 2
- [14] Yuxuan Han, Ruicheng Wang, and Jiaolong Yang. Single-view view synthesis in the wild with learned adaptive multiplane images. In *ACM SIGGRAPH 2022 Conference Proceedings*, pages 1–8, 2022. 1, 2, 3
- [15] Jonathan Ho, Ajay Jain, and Pieter Abbeel. Denoising diffusion probabilistic models. *Advances in neural information processing systems*, 33:6840–6851, 2020. 2, 5
- [16] Julia Hornauer and Vasileios Belagiannis. Gradient-based uncertainty for monocular depth estimation. In *European Conference on Computer Vision*, pages 613–630. Springer, 2022. 4
- [17] Bingxin Ke, Anton Obukhov, Shengyu Huang, Nando Metzger, Rodrigo Caye Daudt, and Konrad Schindler. Repurposing diffusion-based image generators for monocular depth estimation. In *Proceedings of the IEEE/CVF Conference on Computer Vision and Pattern Recognition*, pages 9492–9502, 2024. 2, 3
- [18] Alex Kendall, Hayk Martirosyan, Saumitro Dasgupta, Peter Henry, Ryan Kennedy, Abraham Bachrach, and Adam Bry. End-to-end learning of geometry and context for deep stereo regression. In *Proceedings of the IEEE international conference on computer vision*, pages 66–75, 2017. 2
- [19] Diederik P Kingma. Auto-encoding variational bayes. *arXiv preprint arXiv:1312.6114*, 2013. 3
- [20] Jiankun Li, Peisen Wang, Pengfei Xiong, Tao Cai, Ziwei Yan, Lei Yang, Jiangyu Liu, Haoqiang Fan, and Shuaicheng Liu. Practical stereo matching via cascaded recurrent network with adaptive correlation. In *Proceedings of the IEEE/CVF conference on computer vision and pattern recognition*, pages 16263–16272, 2022. 5, 6
- [21] Zhengqi Li and Noah Snavely. MegadePTH: Learning single-view depth prediction from internet photos. In *Proceedings of the IEEE conference on computer vision and pattern recognition*, pages 2041–2050, 2018. 2
- [22] Zhaoshuo Li, Xingtong Liu, Nathan Drenkow, Andy Ding, Francis X Creighton, Russell H Taylor, and Mathias Unberath. Revisiting stereo depth estimation from a sequence-to-sequence perspective with transformers. In *Proceedings of the IEEE/CVF international conference on computer vision*, pages 6197–6206, 2021. 2
- [23] Haotong Lin, Sida Peng, Jingxiao Chen, Songyou Peng, Jiaming Sun, Minghuan Liu, Hujun Bao, Jiashi Feng, Xiaowei Zhou, and Bingyi Kang. Prompting depth anything for 4k resolution accurate metric depth estimation. In *Proceedings of the Computer Vision and Pattern Recognition Conference*, pages 17070–17080, 2025. 4
- [24] Tsung-Yi Lin, Michael Maire, Serge Belongie, James Hays, Pietro Perona, Deva Ramanan, Piotr Dollár, and C Lawrence Zitnick. Microsoft coco: Common objects in context. In *Computer Vision—ECCV 2014: 13th European Conference, Zurich, Switzerland, September 6–12, 2014, Proceedings, Part V 13*, pages 740–755. Springer, 2014. 6
- [25] Lahav Lipson, Zachary Teed, and Jia Deng. Raft-stereo: Multilevel recurrent field transforms for stereo matching. In *2021 International Conference on 3D Vision (3DV)*, pages 218–227. IEEE, 2021. 1, 2, 6, 8

- [26] Biyang Liu, Huimin Yu, and Guodong Qi. Graftnet: Towards domain generalized stereo matching with a broad-spectrum and task-oriented feature. In *Proceedings of the IEEE/CVF conference on computer vision and pattern recognition*, pages 13012–13021, 2022. 1, 2, 8
- [27] Andreas Lugmayr, Martin Danelljan, Andres Romero, Fisher Yu, Radu Timofte, and Luc Van Gool. Repaint: Inpainting using denoising diffusion probabilistic models. In *Proceedings of the IEEE/CVF conference on computer vision and pattern recognition*, pages 11461–11471, 2022. 2, 6
- [28] Yue Luo, Jimmy Ren, Mude Lin, Jiahao Pang, Wenxiu Sun, Hongsheng Li, and Liang Lin. Single view stereo matching. In *Proceedings of the IEEE conference on computer vision and pattern recognition*, pages 155–163, 2018. 2
- [29] Nikolaus Mayer, Eddy Ilg, Philip Hausser, Philipp Fischer, Daniel Cremers, Alexey Dosovitskiy, and Thomas Brox. A large dataset to train convolutional networks for disparity, optical flow, and scene flow estimation. In *Proceedings of the IEEE conference on computer vision and pattern recognition*, pages 4040–4048, 2016. 1, 2, 3, 5, 7, 8
- [30] Moritz Menze and Andreas Geiger. Object scene flow for autonomous vehicles. In *Proceedings of the IEEE conference on computer vision and pattern recognition*, pages 3061–3070, 2015. 6
- [31] Ben Mildenhall, Pratul P Srinivasan, Matthew Tancik, Jonathan T Barron, Ravi Ramamoorthi, and Ren Ng. Nerf: Representing scenes as neural radiance fields for view synthesis. *Communications of the ACM*, 65(1):99–106, 2021. 1
- [32] Ron Mokady, Amir Hertz, Kfir Aberman, Yael Pritch, and Daniel Cohen-Or. Null-text inversion for editing real images using guided diffusion models. In *Proceedings of the IEEE/CVF conference on computer vision and pattern recognition*, pages 6038–6047, 2023. 1
- [33] Thomas Müller, Alex Evans, Christoph Schied, and Alexander Keller. Instant neural graphics primitives with a multiresolution hash encoding. *ACM transactions on graphics (TOG)*, 41(4):1–15, 2022. 2
- [34] Gerhard Neuhold, Tobias Ollmann, Samuel Rota Buló, and Peter Kotschieder. The mapillary vistas dataset for semantic understanding of street scenes. In *Proceedings of the IEEE international conference on computer vision*, pages 4990–4999, 2017. 6, 1
- [35] Albert Pumarola, Enric Corona, Gerard Pons-Moll, and Francesc Moreno-Noguer. D-nerf: Neural radiance fields for dynamic scenes. In *Proceedings of the IEEE/CVF Conference on Computer Vision and Pattern Recognition*, pages 10318–10327, 2021. 1
- [36] Pierluigi Zama Ramirez, Fabio Tosi, Matteo Poggi, Samuele Salti, Stefano Mattoccia, and Luigi Di Stefano. Open challenges in deep stereo: the booster dataset. In *Proceedings of the IEEE/CVF Conference on Computer Vision and Pattern Recognition*, pages 21168–21178, 2022. 8
- [37] René Ranftl, Katrin Lasinger, David Hafner, Konrad Schindler, and Vladlen Koltun. Towards robust monocular depth estimation: Mixing datasets for zero-shot cross-dataset transfer. *IEEE transactions on pattern analysis and machine intelligence*, 44(3):1623–1637, 2020. 2
- [38] Zhibo Rao, Bangshu Xiong, Mingyi He, Yuchao Dai, Renjie He, Zhelun Shen, and Xing Li. Masked representation learning for domain generalized stereo matching. In *Proceedings of the IEEE/CVF Conference on Computer Vision and Pattern Recognition*, pages 5435–5444, 2023. 1, 2
- [39] Robin Rombach, Andreas Blattmann, Dominik Lorenz, Patrick Esser, and Björn Ommer. High-resolution image synthesis with latent diffusion models. In *Proceedings of the IEEE/CVF conference on computer vision and pattern recognition*, pages 10684–10695, 2022. 2, 3, 5, 1
- [40] Daniel Scharstein, Heiko Hirschmüller, York Kitajima, Greg Krathwohl, Nera Nešić, Xi Wang, and Porter Westling. High-resolution stereo datasets with subpixel-accurate ground truth. In *Pattern Recognition: 36th German Conference, GCPR 2014, Münster, Germany, September 2-5, 2014, Proceedings 36*, pages 31–42. Springer, 2014. 1, 6
- [41] Thomas Schops, Johannes L Schonberger, Silvano Galliani, Torsten Sattler, Konrad Schindler, Marc Pollefeys, and Andreas Geiger. A multi-view stereo benchmark with high-resolution images and multi-camera videos. In *Proceedings of the IEEE conference on computer vision and pattern recognition*, pages 3260–3269, 2017. 1, 6
- [42] Zhelun Shen, Yuchao Dai, and Zhibo Rao. Cfnet: Cascade and fused cost volume for robust stereo matching. In *Proceedings of the IEEE/CVF conference on computer vision and pattern recognition*, pages 13906–13915, 2021. 2, 8
- [43] Jiaming Song, Chenlin Meng, and Stefano Ermon. Denoising diffusion implicit models. *arXiv preprint arXiv:2010.02502*, 2020. 6
- [44] Zachary Teed and Jia Deng. Raft: Recurrent all-pairs field transforms for optical flow. In *Computer Vision—ECCV 2020: 16th European Conference, Glasgow, UK, August 23–28, 2020, Proceedings, Part II 16*, pages 402–419. Springer, 2020. 2
- [45] Alessio Tonioni, Oscar Rahnama, Thomas Joy, Luigi Di Stefano, Thalaisyasingam Ajanthan, and Philip HS Torr. Learning to adapt for stereo. In *Proceedings of the IEEE/CVF Conference on Computer Vision and Pattern Recognition*, pages 9661–9670, 2019. 1
- [46] Alessio Tonioni, Fabio Tosi, Matteo Poggi, Stefano Mattoccia, and Luigi Di Stefano. Real-time self-adaptive deep stereo. In *Proceedings of the IEEE/CVF conference on computer vision and pattern recognition*, pages 195–204, 2019. 1
- [47] Fabio Tosi, Alessio Tonioni, Daniele De Gregorio, and Matteo Poggi. Nerf-supervised deep stereo. In *Proceedings of the IEEE/CVF conference on computer vision and pattern recognition*, pages 855–866, 2023. 2, 6, 7, 8
- [48] Fabio Tosi, Luca Bartolomei, and Matteo Poggi. A survey on deep stereo matching in the twenties. *International Journal of Computer Vision*, pages 1–32, 2025. 1
- [49] Jonathan Tremblay, Thang To, and Stan Birchfield. Falling things: A synthetic dataset for 3d object detection and pose estimation. In *Proceedings of the IEEE conference on computer vision and pattern recognition workshops*, pages 2038–2041, 2018. 6
- [50] Igor Vasiljevic, Nick Kolkin, Shanyi Zhang, Ruotian Luo, Haochen Wang, Falcon Z Dai, Andrea F Daniele, Moham-

- madreza Mostajabi, Steven Basart, Matthew R Walter, et al. Diode: A dense indoor and outdoor depth dataset. *arXiv preprint arXiv:1908.00463*, 2019. 6
- [51] Lezhong Wang, Jeppe Revall Frisvad, Mark Bo Jensen, and Siavash Arjomand Bigdeli. Stereodiffusion: Training-free stereo image generation using latent diffusion models. In *Proceedings of the IEEE/CVF Conference on Computer Vision and Pattern Recognition*, pages 7416–7425, 2024. 5, 6, 7, 1, 2
- [52] Wenshan Wang, DeLong Zhu, Xiangwei Wang, Yaoyu Hu, Yuheng Qiu, Chen Wang, Yafei Hu, Ashish Kapoor, and Sebastian Scherer. Tartanair: A dataset to push the limits of visual slam. In *2020 IEEE/RSJ International Conference on Intelligent Robots and Systems (IROS)*, pages 4909–4916. IEEE, 2020. 1, 5, 6
- [53] Xianqi Wang, Gangwei Xu, Hao Jia, and Xin Yang. Selective-stereo: Adaptive frequency information selection for stereo matching. In *Proceedings of the IEEE/CVF Conference on Computer Vision and Pattern Recognition*, pages 19701–19710, 2024. 1
- [54] Jamie Watson, Oisín Mac Aodha, Daniyar Turmukhambetov, Gabriel J Brostow, and Michael Firman. Learning stereo from single images. In *Computer Vision–ECCV 2020: 16th European Conference, Glasgow, UK, August 23–28, 2020, Proceedings, Part I 16*, pages 722–740. Springer, 2020. 2, 3, 4, 6, 8, 1
- [55] Bowen Wen, Matthew Trepte, Joseph Aribido, Jan Kautz, Orazio Gallo, and Stan Birchfield. Foundationstereo: Zero-shot stereo matching. In *Proceedings of the Computer Vision and Pattern Recognition Conference*, pages 5249–5260, 2025. 6
- [56] Mochu Xiang, Jing Zhang, Nick Barnes, and Yuchao Dai. Measuring and modeling uncertainty degree for monocular depth estimation. *IEEE Transactions on Circuits and Systems for Video Technology*, 2024. 4
- [57] Gangwei Xu, Junda Cheng, Peng Guo, and Xin Yang. Attention concatenation volume for accurate and efficient stereo matching. In *Proceedings of the IEEE/CVF Conference on Computer Vision and Pattern Recognition*, pages 12981–12990, 2022. 1, 2
- [58] Gangwei Xu, Xianqi Wang, Xiaohuan Ding, and Xin Yang. Iterative geometry encoding volume for stereo matching. In *Proceedings of the IEEE/CVF Conference on Computer Vision and Pattern Recognition*, pages 21919–21928, 2023. 2, 6, 8
- [59] Gangwei Xu, Yun Wang, Junda Cheng, Jinhui Tang, and Xin Yang. Accurate and efficient stereo matching via attention concatenation volume. *IEEE Transactions on Pattern Analysis and Machine Intelligence*, 2023. 1
- [60] Gangwei Xu, Xianqi Wang, Zhaoxing Zhang, Junda Cheng, Chunyuan Liao, and Xin Yang. Igev++: Iterative multi-range geometry encoding volumes for stereo matching. *IEEE Transactions on Pattern Analysis and Machine Intelligence*, 2025. 2
- [61] Guorun Yang, Xiao Song, Chaoqin Huang, Zhidong Deng, Jianping Shi, and Bolei Zhou. Drivingstereo: A large-scale dataset for stereo matching in autonomous driving scenarios. In *Proceedings of the IEEE/CVF conference on computer vision and pattern recognition*, pages 899–908, 2019. 2
- [62] Lihe Yang, Bingyi Kang, Zilong Huang, Xiaogang Xu, Jiashi Feng, and Hengshuang Zhao. Depth anything: Unleashing the power of large-scale unlabeled data. In *Proceedings of the IEEE/CVF Conference on Computer Vision and Pattern Recognition*, pages 10371–10381, 2024. 4
- [63] Lihe Yang, Bingyi Kang, Zilong Huang, Zhen Zhao, Xiaogang Xu, Jiashi Feng, and Hengshuang Zhao. Depth anything v2. *Advances in Neural Information Processing Systems*, 37:21875–21911, 2024. 3, 4, 1
- [64] Feihu Zhang, Xiaojuan Qi, Ruigang Yang, Victor Prisacariu, Benjamin Wah, and Philip Torr. Domain-invariant stereo matching networks. In *Computer Vision–ECCV 2020: 16th European Conference, Glasgow, UK, August 23–28, 2020, Proceedings, Part II 16*, pages 420–439. Springer, 2020. 1, 2, 8
- [65] Jiawei Zhang, Jiahe Li, Lei Huang, Xiaohan Yu, Lin Gu, Jin Zheng, and Xiao Bai. Robust synthetic-to-real transfer for stereo matching. In *Proceedings of the IEEE/CVF Conference on Computer Vision and Pattern Recognition*, pages 20247–20257, 2024. 8
- [66] Lvmin Zhang, Anyi Rao, and Maneesh Agrawala. Adding conditional control to text-to-image diffusion models. In *Proceedings of the IEEE/CVF International Conference on Computer Vision*, pages 3836–3847, 2023. 2
- [67] Yongjian Zhang, Longguang Wang, Kunhong Li, Yun Wang, and Yulan Guo. Learning representations from foundation models for domain generalized stereo matching. In *European Conference on Computer Vision*, pages 146–162. Springer, 2024. 8
- [68] Bolei Zhou, Hang Zhao, Xavier Puig, Sanja Fidler, Adela Barriuso, and Antonio Torralba. Scene parsing through ade20k dataset. In *Proceedings of the IEEE conference on computer vision and pattern recognition*, pages 633–641, 2017. 6
- [69] Tinghui Zhou, Richard Tucker, John Flynn, Graham Fyffe, and Noah Snavely. Stereo magnification: Learning view synthesis using multiplane images. *arXiv preprint arXiv:1805.09817*, 2018. 1

ZeroStereo: Zero-shot Stereo Matching from Single Images

Supplementary Material

Method	KITTI-15		Midd-T (H)		ETH3D	
	EPE	>3px	EPE	>2px	EPE	>1px
\mathcal{L}_p	1.03	4.77	0.90	4.95	0.25	2.09
$(1 - C) \odot \mathcal{L}_p$	1.03	4.76	0.85	4.81	0.25	2.08
$(1 - C) \odot \mathcal{L}_{np}$	1.02	4.53	0.79	4.45	0.23	2.13

Table 9. Analysis of ZeroStereo loss (trained with RAFT-Stereo [25]). We discuss the loss combinations based on \mathcal{L}_d .

6. Details of Image Synthesis

Image Resolution. The input resolution of Depth Anything V2 [63] and Stable Diffusion V2 Inpainting [39] is constrained, which may lead to object deformation when resizing images. To address this, we apply padding operations to adjust image dimensions while preserving their original aspect ratio. For example, when using Depth Anything V2, we pad images to ensure their height and width are divisible by 14. Additionally, high-resolution images, particularly those from the Mapillary Vistas [34], may exceed available GPU memory during inference. To mitigate this issue, we first downscale images proportionally to half or quarter of their original resolution, perform inference, and then up-scale the outputs to restore the original dimensions.

Forward Warping. We utilize the source code of MfS-Stereo [54] to implement forward warping, including non-occlusion computation and depth sharpening. However, when applying a diffusion model for inpainting, we identify several challenges. First, despite advancements in monocular depth estimation, depth edges do not always align precisely with object boundaries. As a result, after forward warping, the edges of foreground objects may remain in their original positions. Second, the proximity between the inpainting mask and the warped foreground objects can mislead the diffusion model during inference. To mitigate these issues, we employ a simple yet effective approach: using the dilate function in OpenCV to inflate the pseudo-disparity map. This operation ensures that foreground objects and nearby background pixels move together during forward warping. Consequently, during inpainting, background pixels act as a buffer between the mask and the foreground, reducing misleading information. However, despite this refinement, the pre-trained diffusion model still produces ghosting artifacts and noise in many cases (Fig. 5). These artifacts can only be effectively addressed by fine-tuning the diffusion model.

7. Loss Analysis

In Sec. 3.5, we introduce the non-occlusion photometric loss \mathcal{L}_{np} and the weighted final loss \mathcal{L}_{Zero} . However, their

Method	AbsErr ↓	SSIM ↑	\mathcal{L}_p ↓
StereoDiffusion [51]	0.082	0.269	0.323
Ours	0.025	0.850	0.068

Table 10. Reconstruction loss. We warp the synthesized right image with the pseudo disparity and compare it with the left image.

specific impact on stereo training has not been explicitly analyzed. As shown in Tab. 9, the methods listed from top to bottom correspond to: (1) applying the ordinary photometric loss \mathcal{L}_p , (2) using \mathcal{L}_p with the weight $1 - C$, and (3) employing \mathcal{L}_{np} with the weight $1 - C$.

Among these, \mathcal{L}_p alone yields the worst performance across all datasets due to the absence of balanced weighting and its inability to handle ghost artifacts and inpainting pixels. Introducing the weight $1 - C$ mitigates these issues, leading to improved performance. The best results are achieved when masks are further applied to filter out ghost artifacts and inpainting pixels, highlighting the effectiveness of our proposed approach.

8. Discussion on Synthesis Methods

In this section, we discuss two synthesis methods: StereoDiffusion [51] and AdaMPI [14].

StereoDiffusion [51] is a training-free method that utilizes a pre-trained latent diffusion model to generate stereo pairs from a single image. It applies null-text inversion [32] for image editing, first reversing the diffusion process to obtain a latent representation of the input image and then applying forward diffusion to synthesize the right view. However, this approach has notable limitations. First, inference is computationally expensive. As shown in Tab. 4, synthesizing a 512×512 image takes approximately 30 seconds. Second, the null-text inversion process can unintentionally modify the left image, introducing content inconsistencies. As illustrated in Fig. 9, the original image lacks stones, yet both the generated left and right views erroneously include them. Similarly, fine details such as text often become distorted. Quantitative reconstruction loss measurements (Tab. 10) confirm these issues, showing significantly higher errors compared to our method. Moreover, using StereoDiffusion-generated stereo pairs for training stereo matching networks led to poor performance and convergence difficulties.

AdaMPI [14] generates multiplane images [69] (MPI) from a single input image from a single input image for novel view synthesis. However, as shown in Fig. 10, varying the camera motion ratios often introduces artifacts, particularly in occluded regions, where ghosting and trailing effects are prevalent. This suggests that the MPI approach

Method	Cloudy		Foggy		Rainy		Sunny	
	F	H	F	H	F	H	F	H
NS-RAFT-Stereo	8.81	2.95	18.18	3.41	29.19	8.47	7.42	2.88
Zero-RAFT-Stereo	6.44	2.69	8.66	1.70	30.10	11.71	6.46	3.15

Table 11. Zero-shot generalization performance on DrivingStereo under different weather. We utilize $>3\text{px}$ All in comparisons.

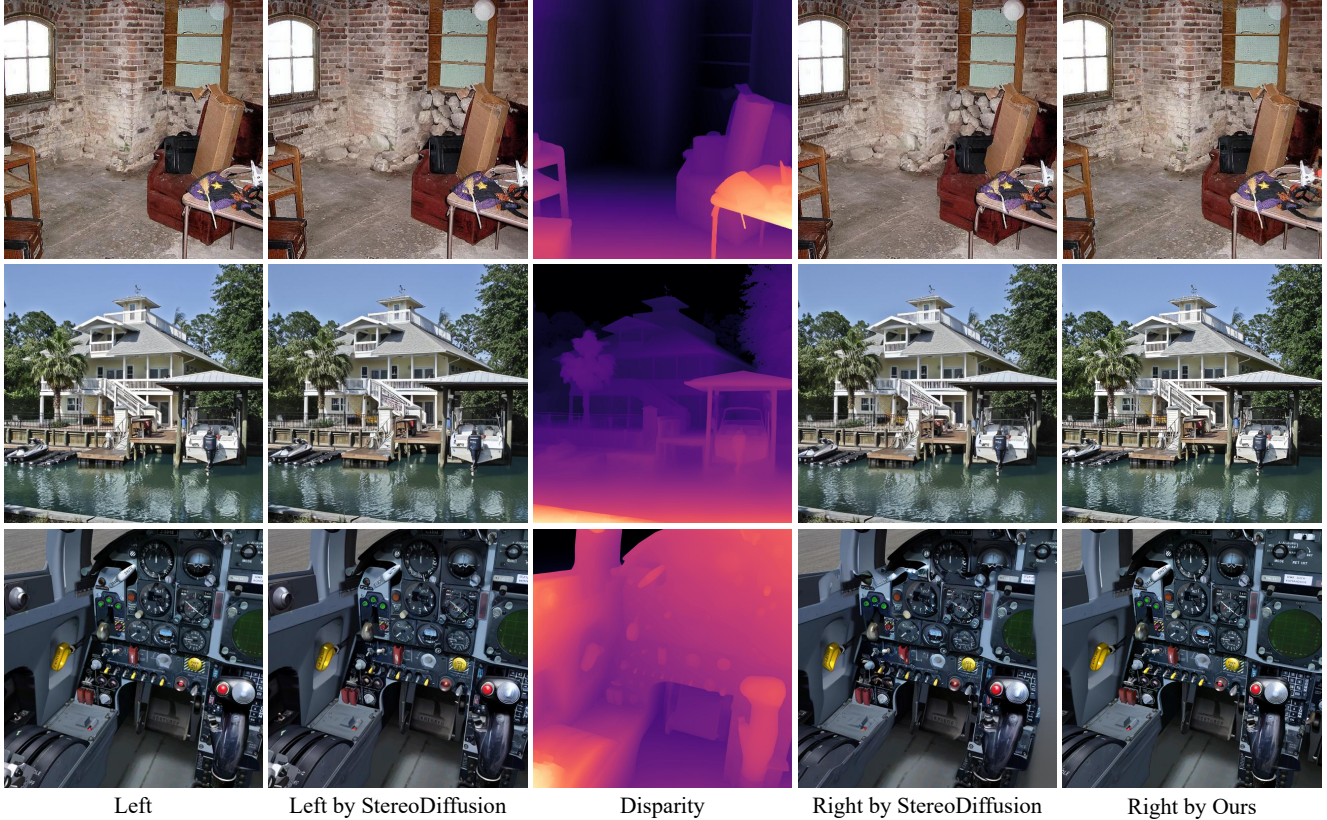


Figure 9. Visualization of StereoDiffusion [51].

struggles to reconstruct the scene’s semantic structure accurately. As a result, MPI-based stereo generation is less suitable for training stereo matching models, as these artifacts compromise the quality and consistency needed for effective learning.

In summary, while StereoDiffusion [51] and AdaMPI [14] introduce innovative approaches for synthesizing stereo images from single inputs, both have significant limitations. StereoDiffusion suffers from high computational costs and content distortions, while AdaMPI struggles with semantic inconsistencies in occluded regions. These challenges highlight the need for more robust and accurate synthesis methods for stereo matching applications.

9. Additional Comparisons with NeRF-Stereo

In this section, we present additional comparisons with NeRF-Stereo [47], detailed Midd-T benchmark results, vi-

sualizations on KITTI and ETH3D, and zero-shot generalization performance on DrivingStereo [61].

For Midd-T, we report the performance of each sample in Tab. 12. Compared to NS-RAFT-Stereo [47], our Zero-RAFT-Stereo achieves improvements in nearly all cases. Notably, for samples where NS-RAFT-Stereo performs poorly, our method improves accuracy by almost 50%.

For KITTI and ETH3D, we provide visual comparisons between NS-RAFT-Stereo and Zero-RAFT-Stereo. As shown in Fig. 11, Fig. 12, Zero-RAFT-Stereo generates smoother and more accurate disparity maps with fewer artifacts and reduced noise. Notably, in the second row of Fig. 12, our model effectively removes the large disparity artifacts present in NS-RAFT-Stereo, particularly in the central dark region, demonstrating its superior handling of challenging textures and illumination variations.

Additionally, we evaluate both models on the DrivingStereo dataset under different weather conditions. As

Method	Adi.	ArtL	Jad.	Mot.	Mot.E	Pia.	Pia.L	Pip.	Plr.	Plt.	Plt.P	Rec.	She.	Ted.	Vin.
NS-RAFT-Stereo	1.51	4.14	24.90	3.62	4.04	9.04	25.81	5.89	14.08	6.13	5.54	4.94	39.59	4.96	26.35
Zero-RAFT-Stereo	1.39	4.91	14.27	3.26	3.68	5.69	13.73	5.22	9.53	7.21	5.50	4.20	23.97	4.77	18.01

Table 12. Details of Midd-T. We utilize $>2\text{px}$ Noc regions in Midd-T (F)

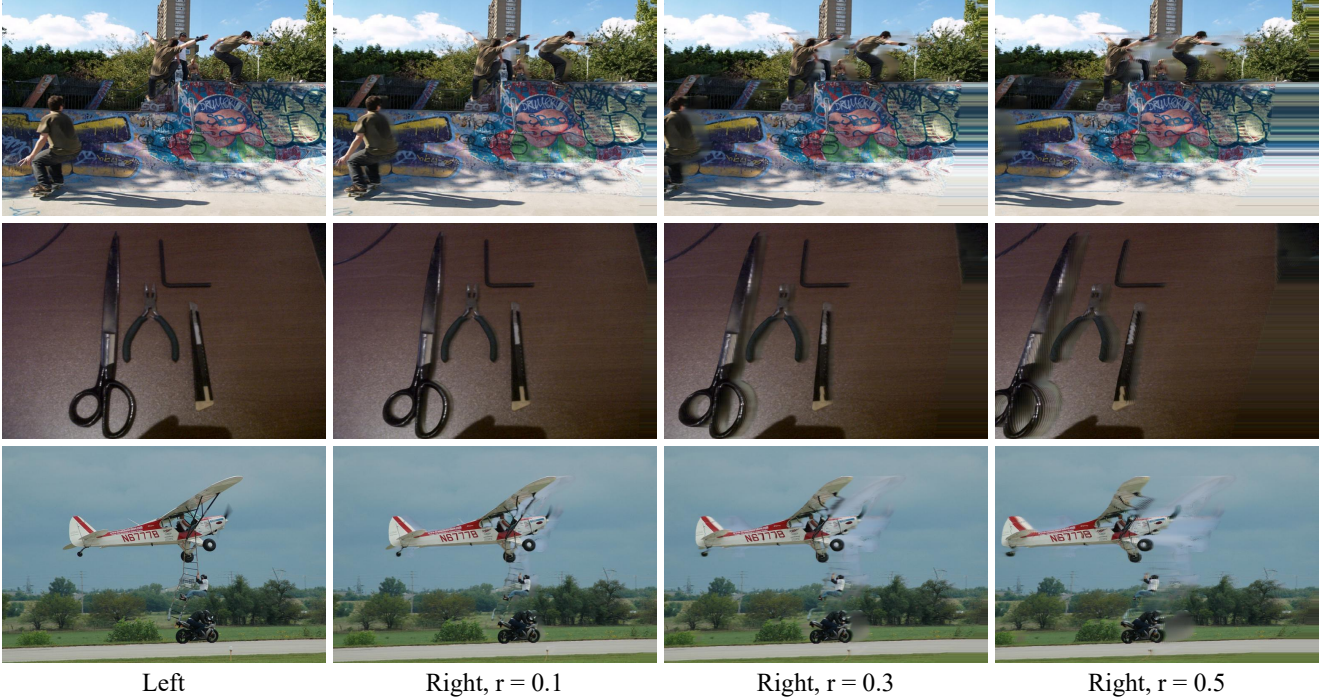


Figure 10. Visualization of AdaMPI [14].

shown in Tab. 11, our Zero-RAFT-Stereo outperforms NS-RAFT-Stereo across all weather conditions except rainy weather, where both models exhibit poor performance, indicating a need for further optimization in such scenarios. Notably, Zero-RAFT-Stereo demonstrates significant improvements under foggy conditions, reducing errors from 18.18% to 8.66% at full resolution and from 3.41% to 1.70% at half resolution. Since foggy scenes typically have low contrast and poor visibility, these results suggest that Zero-RAFT-Stereo is more robust in such challenging conditions. As illustrated in Fig. 13, under extreme weather conditions, NS-RAFT-Stereo struggles to predict large textureless regions, while Zero-RAFT-Stereo successfully reconstructs complete ground surfaces and walls. Moreover, Zero-RAFT-Stereo exhibits superior segmentation of thin, tree-like objects and blurry background regions, highlighting its ability to maintain fine details even in adverse conditions.

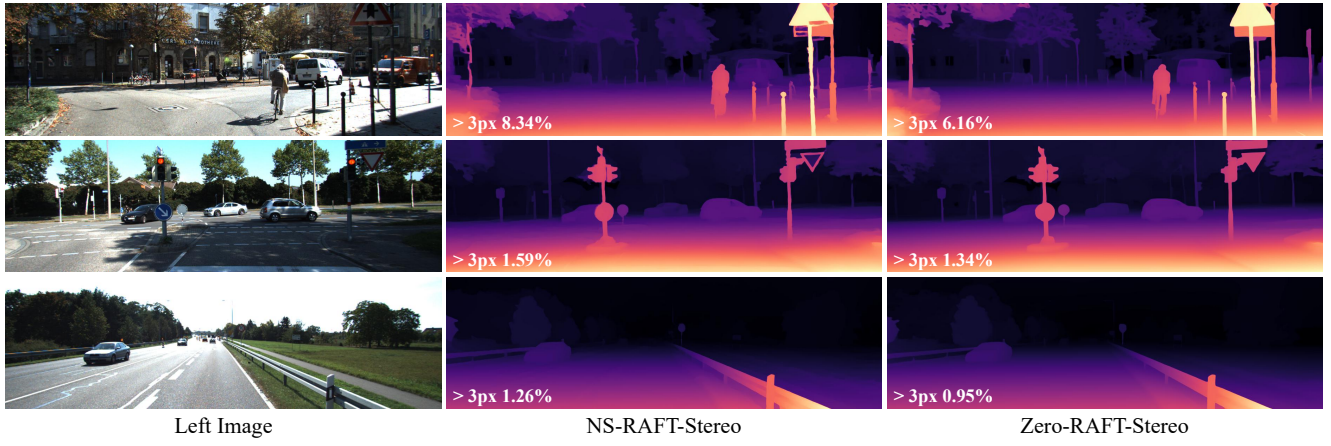


Figure 11. Visualization of KITTI.

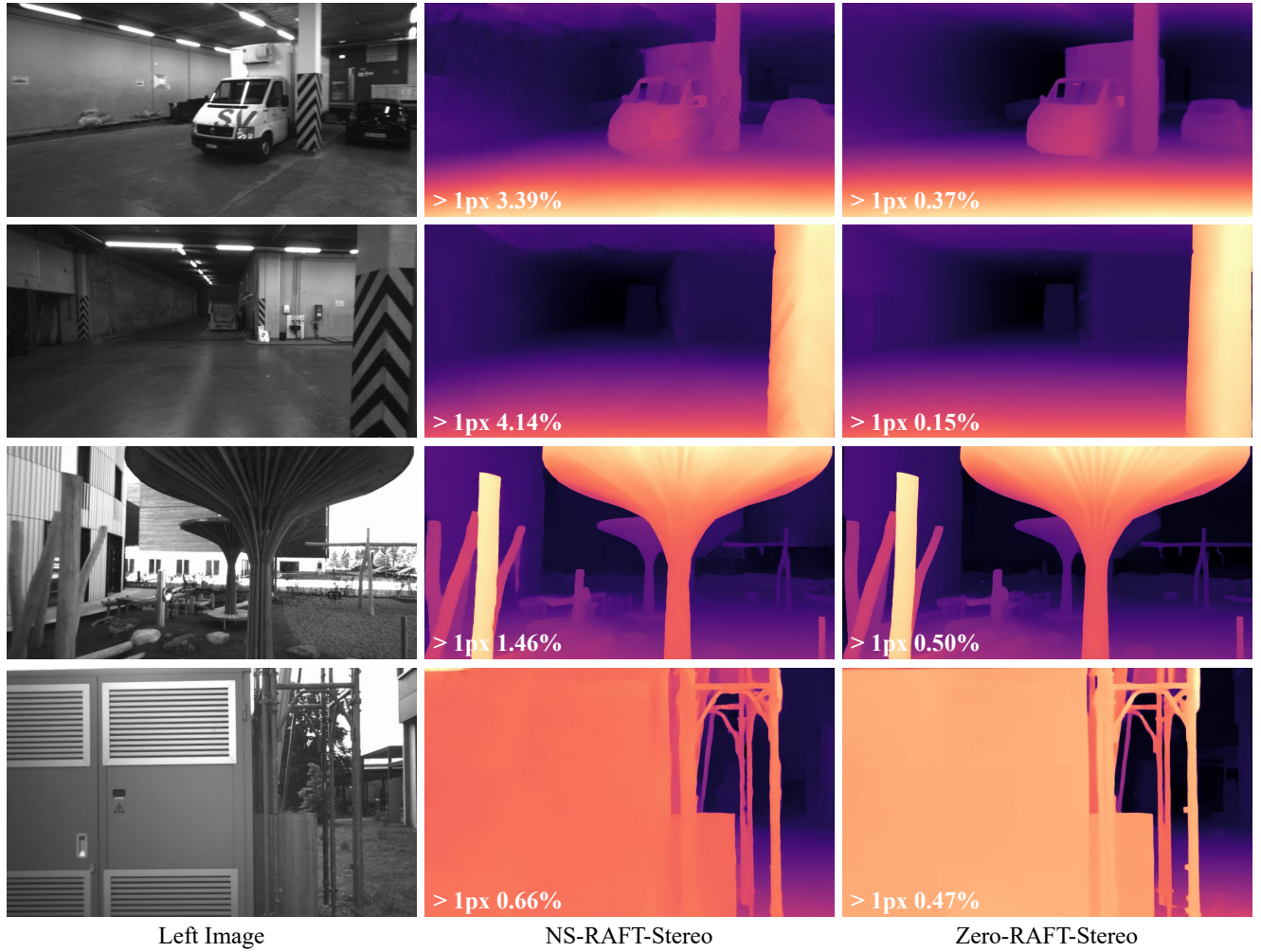


Figure 12. Visualization of ETH3D.

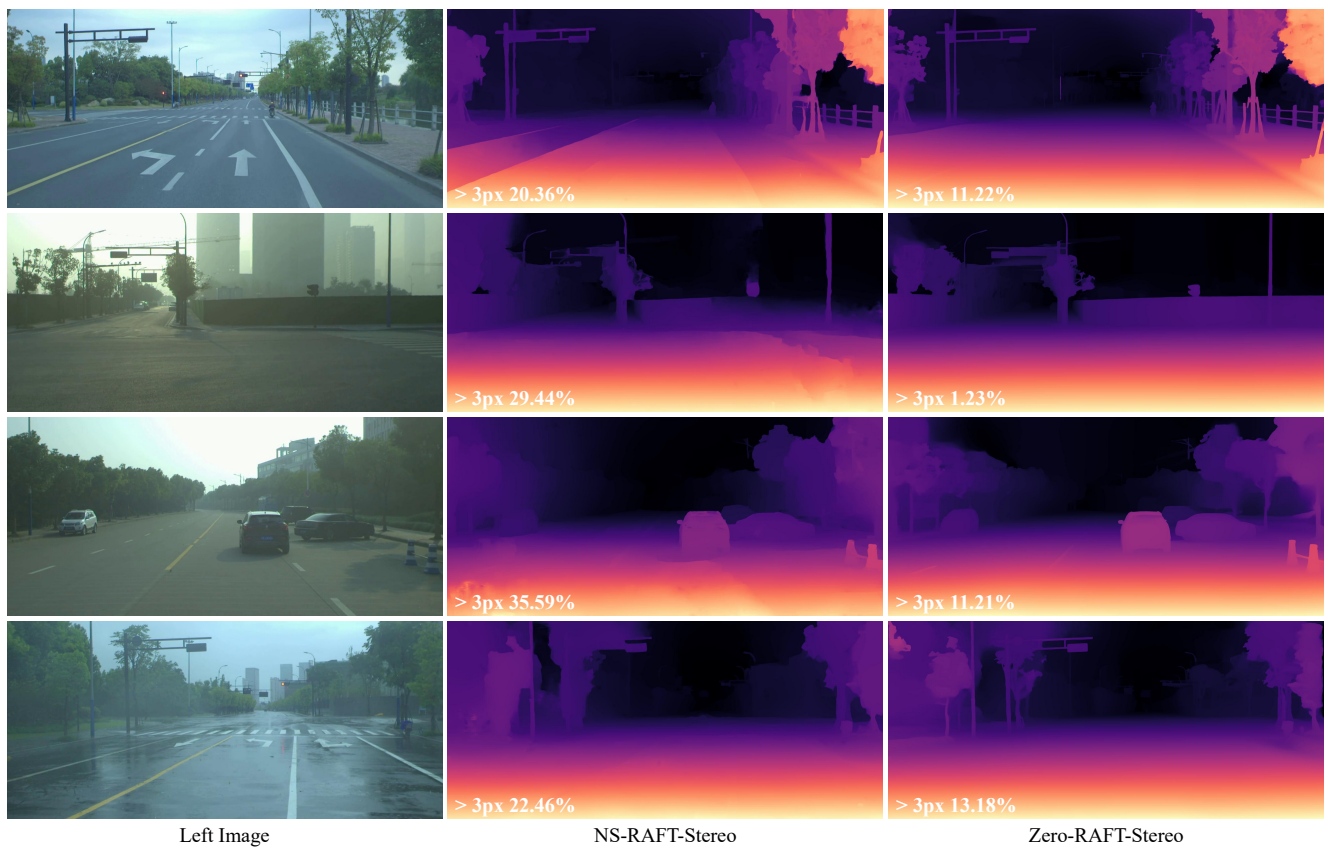


Figure 13. Visualization of DrivingStereo.